



Numerical Study of Kelvin-Helmholtz Instability of Newtonian and Non-Newtonian Fluids

R. Farajzadeh, M. Bayareh*

Department of Mechanical Engineering, Shahrekord University, Shahrekord, Iran

ABSTRACT: Kelvin-Helmholtz instability is a hydrodynamic instability generated by the relative motion of immiscible, irrotational, incompressible, and inviscid fluids. In the present study, the Kelvin-Helmholtz instability is assessed for Newtonian and non-Newtonian fluids by solving two-dimensional Navier-Stokes equations using the finite volume method. ANSYS FLUENT software is used to simulate the two-phase flow field. The numerical method is the finite volume method. Using the semi-implicit method for pressure-linked equations algorithm, the velocity and pressure fields are coupled and the Navier-Stokes equations are solved. The second-order upwind method is used to discretize the convection terms in Navier-Stokes equations and the central difference method is employed to approximate the time derivative. In the case of Newtonian fluids, it was found that for $t^* > 1.5$ the growth rate of Kelvin-Helmholtz instability depends on the surface tension when the surface tension is in the range of 0.000192-0.000993 N/m. The results demonstrate that the critical wavenumber is enhanced by increasing the power-law index (n) for shear-thinning and shear-thickening non-Newtonian fluids; however, at a specific time, the amount of critical wavenumber for shear-thickening fluids is smaller than that for shear-thinning ones. It is also concluded that as the power-law index increases, the wave stability can be reached more rapidly.

Review History:

Received: Aug. 07, 2021

Revised: Oct. 16, 2021

Accepted: Dec. 21, 2021

Available Online: Dec. 26, 2021

Keywords:

Kelvin-Helmholtz instability

Two-phase flow

Non-Newtonian fluids

Surface tension

1- Introduction

Low-viscosity flows become turbulent faster than the high-viscosity ones. In some cases, the flow instabilities intensify until the flow becomes turbulent. For example, if a layer of heavy fluid, such as water, moves over a layer of lighter fluid, such as oil, the instability called Rayleigh-Taylor Instability (RTI) is created, leading to flow turbulence. Another type of instability called Kelvin-Helmholtz Instability (KHI) occurs when two layers of fluid move in opposite directions with different velocities. This condition can also cause disturbances in the interface of fluids. The main mechanism for the development of KHI is the existence of a uniform shear that does not require gravity or density difference. Therefore, these effects, as well as surface tension and viscosity, are often not considered in numerical studies to simplify the calculations [1].

KHI was first studied by Hermann von Helmholtz [2] and William Thomson (Lord Kelvin) [3] and the linear stability was numerically studied by Hazel [4]. Thorpe's group [5-9] investigated the KHI by tilting a tube containing two liquids of different densities. Their experiment [7] consisted of a glass channel containing two different incompressible liquids of similar density. The liquids were water and a mixture of commercial tetrachloride and paraffin. Initially, the tube was filled with both liquid layers with the same initial height. Once

the fluids were settled, the channel tilted at an angle of $\sin \alpha = 0.072$, resulting in the motion of a wavy flow that caused the KHI to form. Unverdi and Tryggvason [10] described a method for simulating unstable multi-phase flows in which a critical interface separates incompressible liquids of different densities and viscosities. The flow field was discretized with a finite difference approximation on a stationary grid, and the interface was explicitly represented by a separate unstructured grid moving through a fixed one. Gondret and Rabaud [11] experimentally investigated the parallel flow of two immiscible liquids in a Hele-Shaw cell and reported that the instability threshold in the liquid-liquid interface is controlled by inertial force, while the wave velocity and its growth rate are controlled by the viscosity. Mohammadi Masiri et al. [12] investigated the impact of non-Newtonian fluid flow on the interaction between two drops using the front tracking method. This technique can be employed to model the interface. Terashima and Tryggvason [13] introduced a front-tracking method to simulate the interface of a fluid in a compressible flow. Their results revealed that their method can simulate multiphase flows for a wide range of compression ratios and surface tension. Wang et al. [14] studied the numerical nonlinear evolution of KHI with and without thermal conductivity and demonstrated that the growth of KHI of small-scale structures is reduced with thermal conductiv-

*Corresponding author's email: m.bayareh@sku.ac.ir



ity while the vortex coupling process is enhanced. Chen and Forbes [15] modeled the KHI for inviscid and viscous liquids that were parallel to each other using a spectral method and a finite difference scheme. They showed that the convergence of the viscous model depends on the quasi-time step strongly. Yilmaz et al. [16] calculated the growth rate of instability in KHI using a DNS algorithm and demonstrated that the interface of compressible fluids is unstable when much number is equal to or less than one. Zhang et al. [17] studied two-dimensional KHI using a lattice Boltzmann multi-phase model for incompressible fluids and expressed that the contribution of surface stress to the kinetic energy and flow enstrophy is negative and positive, respectively. Their results showed that the nonlinear behavior of the two-phase combination is affected by surface tension. As the surface tension increases (the capillary number decreases), the flow field interactions become more intense. Shadloo and Yildiz [18] investigated the effects of Richardson number and density ratio on the development of KHI of two incompressible, immiscible, and inviscid liquids using the smooth particle hydrodynamics method and observed that the total growth rate of KHI is largely controlled by the value of the Richardson number. Kumar Awaṣṡhi and Agrawal [19] studied the contribution of viscosity to pressure to analyze the KHI of viscous potential flow with a tangential magnetic field at the interface of two viscous liquids and observed that irrotational shear stresses have a constant effect on system stability. Shiryeva et al. [20] analyzed an ideal model of two incompatible liquids so that bottom and top viscous liquids moved at a constant velocity parallel to the interface. They showed that the viscosity of the two liquids reduces the damping of the waves on the interface. Matsson and Boisselle [21] developed and tested the KHI and showed that the instability is developed for 3 seconds when the tube was tilted 8 degrees relative to the horizontal axis.

For the case of Newtonian fluids, the KHI is affected by surface tension, fluid velocity, heat transfer rate, fluids viscosity, fluid thermal conductivity, and fluid density. Even though the stability of non-Newtonian fluids is pivotal in practical applications, a few investigators have assessed the stability of the non-Newtonian liquid-liquid (gas) interface. For instance, Awaṣṡhi [22] utilized the Oldroyd-B model to analyze the impact of heat and mass transfer on the KHI of the viscoelastic liquid-viscous gas interface. It was demonstrated the range of stable wave numbers is reduced when heat transfer is enhanced. Fu et al. [23] used the same model and confirmed the conclusions of Awaṣṡhi [22]. Besides, they showed that the maximum growth rate increases with the Reynolds number. Ghazanfarian and Moradi [24] employed Smoothed-Particle Hydrodynamics (SPH) and Molecular Dynamics (MD) and proposed a new KHI with three layers of parallel flow. They observed that the stability of the water-water interface is smaller than the water-air interface. Esmailpour and Gholami Korzani [25] evaluated the impact of the power-law index on the interfacial instability of fluids. They found that the finger structure is affected by buoyancy, inertial, and viscous

forces. Vadivukkarasan [26] examined the combined impact of Rayleigh-Taylor instability (RTI) and KHI of an inviscid cylindrical interface and concluded that the Bond number can predict the growth rate and axial wavenumber appropriately.

Although the dynamics of KHI for Newtonian and even viscoelastic fluids have been described, the displacement of non-Newtonian fluid by another one has not been analyzed. To the best of the authors' knowledge, the stability of shear-thinning and shear-thickening fluids is considered in the current study for the first time. The present study aims to study KHI for non-Newtonian liquids using ANSYS FLUENT software numerically. Liquids are assumed to be incompressible and immiscible and the flow is unsteady. The effect of different parameters on KHI is investigated for shear-thinning and shear-thickening fluids. The rest of the paper is organized as follows: Sec. 2 presents the equations that govern the problem. The numerical method is described in Sec. 3, and Sec. 4 provides the results, including grid study, verification, and discussions. Finally, concluding remarks are presented in Sec. 5.

2- Governing Equations

The geometry of the present problem is shown in Fig. 1. Two immiscible liquid streams are in contact with each other. The top liquid has the density and viscosity of ρ_1 and μ_1 , respectively, and moves with the velocity of U_1 . The bottom one has the density and viscosity of ρ_2 and μ_2 , respectively, and has the velocity of U_2 . These two velocities with opposite directions are caused by the tilt of the enclosure.

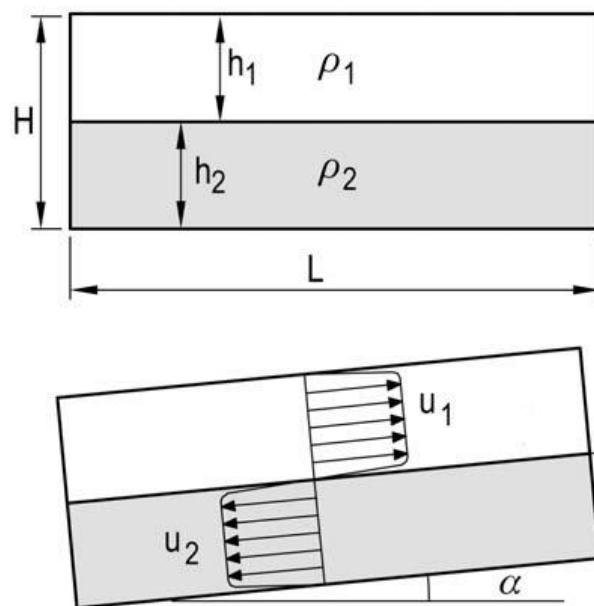


Fig. 1. Schematic of the present problem, $L = 2.4$ m and $H = 0.2$ m.

The continuity and momentum equations for an incompressible and immiscible fluid flow are as follows [17] :

$$\nabla \cdot \mathbf{u} = 0 \tag{1}$$

$$\rho \frac{\partial \mathbf{u}}{\partial t} + \rho \nabla \cdot (\mathbf{u}\mathbf{u}) = -\nabla P + \nabla \cdot \boldsymbol{\tau} + \mathbf{F}_s \tag{2}$$

where \mathbf{u} is the velocity vector, ρ is the density, p is the pressure, $\boldsymbol{\tau}$ is shear stress, and \mathbf{F}_s is the force due to surface tension [27]. The surface tension model used in the simulations is the Continuous Surface Force (CSF) model:

$$\mathbf{F}_s = \sigma \mathbf{k} \nabla \alpha \tag{3}$$

where α is the volume fraction defined as the ratio of the volume of each phase to the cell volume. Surface tension is calculated on the interface and is perpendicular to the surface. The curvature of the interface is calculated as follows:

$$\mathbf{k} = \nabla \cdot \frac{\nabla \alpha}{|\nabla \alpha|} \tag{4}$$

The power-law model is used to evaluate the KHI of shear-thinning ($n < 1$), shear-thickening ($n > 1$), and Newtonian fluids ($n = 1$), where n is the power-law index:

$$\boldsymbol{\tau} = k \dot{\gamma}^n \tag{5}$$

In this equation, k is the flow consistency index. The strain tensor $\dot{\gamma}$ is defined as follows:

$$\dot{\gamma} = (\nabla \mathbf{u}) + (\nabla \mathbf{u})^T \tag{6}$$

Time and velocity scales are introduced as follows to normalize the velocity and time [28]:

$$\begin{aligned} \tilde{\tau} &= \frac{1}{\kappa \Delta U} \\ \tilde{U} &= \Delta U \end{aligned} \tag{7}$$

where $\Delta U = U_2 - U_1$ and $\kappa = 2\pi/\lambda$ is the wavenumber.

Besides, the Reynolds number is determined based on the properties of top and bottom liquids, respectively, as

$$\begin{aligned} Re_1 &= \frac{\rho_1 \Delta U h_1}{\mu_1} \\ Re_2 &= \frac{\rho_2 \Delta U h_2}{\mu_2} \end{aligned} \tag{8}$$

Also, the density and viscosity ratios are defined as follows, respectively:

$$r = \frac{\rho_1}{\rho_2} \tag{9}$$

$$m = \frac{\mu_1}{\mu_2} \tag{10}$$

3- Numerical Method

The assumptions used in the present simulations are as follows:

- Newtonian/non-Newtonian fluids are incompressible.
- Fluid flow is considered to be fully developed.
- Fluids are immiscible.
- At the interface between the two fluids, no phase change occurs.

Fluid properties including density, surface tension, and viscosity are assumed to be constant.

Since the density and viscosity of the two fluids are different, the material derivative of density and viscosity of each fluid particle is assumed to be zero to track their evolution by state equations. To determine the situation of the interface between the different phases, a marker function is used to reconstruct the phase boundary. Thus, the Volume Of Fluid (VOF) approach is employed to simulate the KHI of Newtonian and non-Newtonian fluids. An indicator function, i.e. volume fraction, is used to characterize the two phases. Thus, the density and viscosity of each phase can be determined as follows [29]:

$$\rho(x, t) = \rho_1 \alpha + \rho_2 (1 - \alpha) \tag{11}$$

$$\mu(x, t) = \mu_1 \alpha + \mu_2 (1 - \alpha) \tag{12}$$

In the VOF method, the volume fraction follows the following pattern, when the cell is occupied by liquid phase: $\alpha = 1$, when the cell includes the interface: $0 < \alpha < 1$, and when the cell is occupied by air phase: $\alpha = 0$. α is calculated using Eq. (13) [30]:

$$\frac{\partial \alpha}{\partial t} + \mathbf{u} \cdot \nabla \alpha = 0 \tag{13}$$

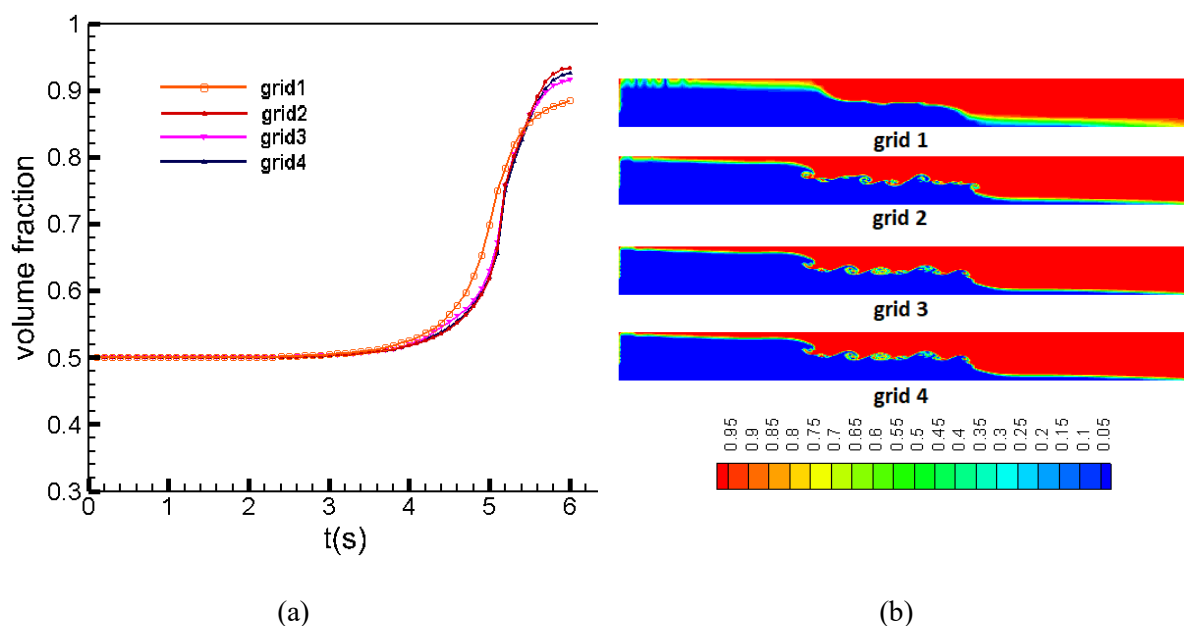


Fig. 2. (a) Water volume fraction versus time for different grid resolutions, (b) concentration contours for different grid resolutions when $r = 0.93$, $m = 0.79$, $Re_1 = 1.49$, and $Re_2 = 1.19$.

In the present work, ANSYS FLUENT software is used to simulate the two-phase flow field. The numerical method is the finite volume method. Using the Semi-Implicit Method for Pressure-Linked Equations (SIMPLE) algorithm, the velocity and pressure fields are coupled and the Navier-Stokes equations are solved. The second-order upwind method is used to discretize the convection terms in Navier-Stokes equations and the central difference method is employed to approximate the time derivative. Besides, the volume fraction is modeled using the Geo-Reconstruct method. To begin with instability, a small disturbance is applied to the interface using a user-defined code. MATLAB software is employed to analyze the results since the output of the Fourier transform for spatial data is wave number and for temporal data is frequency. The interface data is given to MATLAB software to plot the wavenumber of spatial data and obtain the wavenumber. Then, the relevant diagrams are drawn using the Tecplot software. Besides, it should be pointed out that the convergence criterion is 10^{-7} .

4- Results

In this section, the KHI of Newtonian and non-Newtonian fluids flowing in a two-dimensional rectangular cavity is investigated. First, the validation of the results and the independence of the solution from the number of grid points are investigated. Then, the KHI of Newtonian and non-Newtonian fluids is analyzed for different conditions.

4- 1- Grid study

The results of the numerical solution must be independent of the number of cells used in the computational domain. The number of cells must be sufficient on the one hand to capture the hydrodynamics of the fluid flow, and on the other hand to

reduce the computational cost by determining a reasonable minimum number of cells. Hence, the water volume fraction is calculated using four computational grids (grids 1 to 4). Grid 1, grid 2, grid 3, and grid 4 have 4800, 14700, 19200, and 30,000 cells, respectively. Fig. 2a shows that the change in computational grid size has a small effect on the simulations. According to this figure, the grid resolution of 19200 is selected for further simulations. Besides, Fig. 2b compares the volume fraction of liquids for different grid resolutions and demonstrates that the thickness of the interface is reasonable for grid 3 and grid 4.

4- 2- Validation

To verify the present simulations, the numerical results of Tauber et al. [28] and experimental data of Thorpe [6] are employed. Tauber et al. [28] evaluated the breakup of immiscible fluids' interface using the front-tracking approach at finite Reynolds numbers. The fluids were moving with different velocities in opposite directions (like Fig. 1). The top and the bottom walls are rigid and the sidewalls have a periodic boundary condition when H is twice the wavelength and L is equal to the wavelength. The amplitude normalized by the wavelength is plotted in Fig. 3a when the density ratio is unity and $we = (\rho_2 \Delta U^2) / (\sigma \kappa = 6)$. According to linear theory, the wave growth is rapidly for a dimensionless time less than 30. As the finger structure stops growing, the amplitude is reduced. Fig. 3a demonstrates that the present simulations can predict the variations of normalized amplitude at different non-dimensional times.

Qualitatively, the present results are compared with the experimental observations of Thorpe [6], who investigated the instability of stratified shear flows. It was reported that the system is unstable when

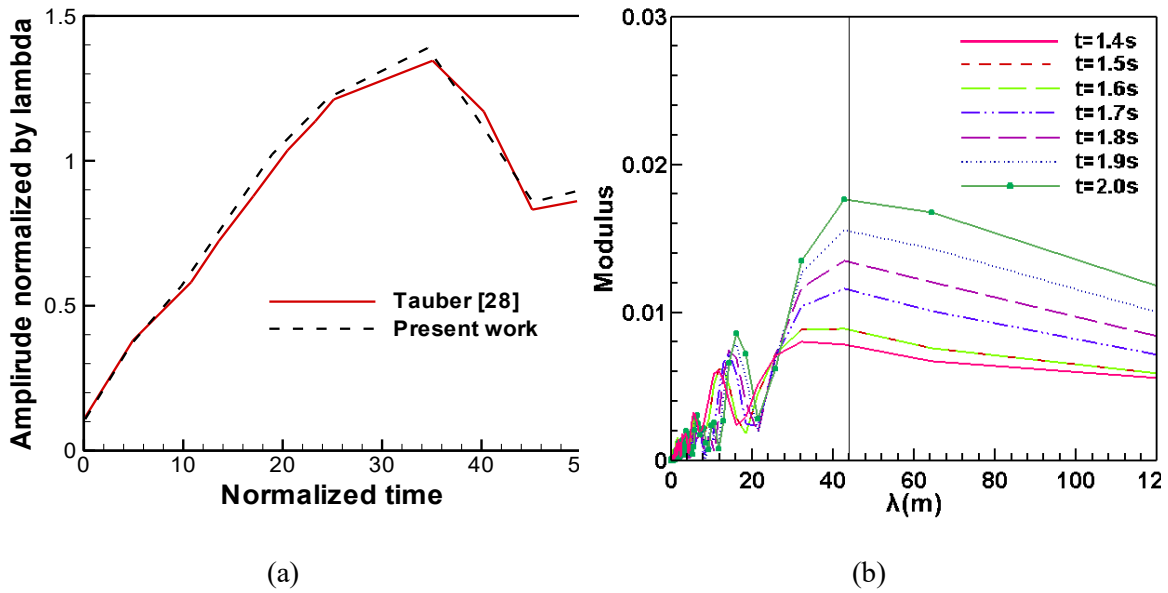


Fig. 4. (a) Normalized amplitude versus dimensionless time for $r = 1$, $Re_1 = 5000$, and $Re_2 = 10000$, and $We = 6$, (b) Fourier analysis of horizontal velocity at the interface between $t = 1.4$ s and $t = 3.0$ s for $r = 0.93$, $m = 0.79$, $Re_1 = 1.49$, and $Re_2 = 1.19$.

Table 1. Properties of Newtonian fluids.

Water		Saltwater	
ρ_1 (kg/m ³)	ν_1 (m ² /s)	ρ_2 (kg/ m ³)	ν_2 (m ² /s)
998.2	0.001002	1074.79	0.001259

$$\Delta U > \frac{\rho_1 + \rho_2}{\rho_1 \rho_2} \left[\sigma \kappa + \frac{g}{\kappa} (\rho_1 + \rho_2) \right] \tanh(\kappa H) \quad (14)$$

Critical magnitudes of wavelength and wavenumber can be estimated as follows, respectively:

$$\kappa_{cr} = \sqrt{\frac{g(\rho_1 + \rho_2)}{\sigma}} \quad (15)$$

$$\lambda_{cr} = \frac{2\pi}{\kappa_{cr}} \quad (16)$$

Fig. 3b shows the Fourier analysis of horizontal velocity at the interface between $t = 1.4$ s and $t = 3$ s. Fourier transforms are obtained using the Fast Fourier Transform (FFT) algorithm. The figure reveals that the onset time of instability is $1.6 < t < 1.7$ s because the growth rate between these values is considerable. This is consistent with the results of Thorpe [6]. Besides, the critical wavelength is measured as $\lambda_{cr} = 44$ mm when critical wave number is $\kappa_{cr} = 142.8$ m. This value was reported by Thorpe [6] in the range of 25-45 mm when $\kappa_{cr} = 197 \pm 58$ m. Thus, the calculated values are in agreement with the results of Thorpe [6].

4- 3- KHI of Newtonian fluids ($n = 1$)

In this section, the evolution of the interface between water and saltwater is considered, where their density and kinematic viscosity are presented in Table 1.

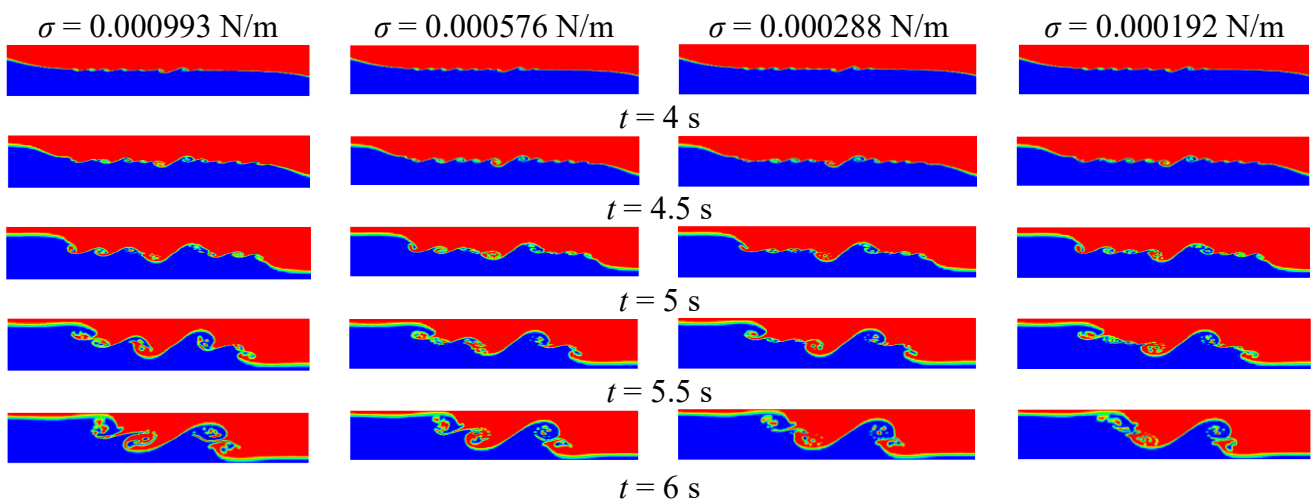


Fig. 4. Time evolution of concentration contours for different surface tension coefficients $r = 0.93$, $m = 0.79$, $Re_1 = 1.49$, and $Re_2 = 1.19$.

4- 3- 1- Effect of surface tension

Fig. 4 shows the time evolution of concentration contours for different surface tension coefficients. When $\sigma = 0.000993$ N/m, the initial disturbance grows rapidly and the wave becomes steeper in the early stages. The peak moves clockwise inward, creating vortices inside the wave. Besides, the shear layer thickness is increased due to the adhesive diffusion. The separation of the vertex from the wave peak, which can be observed at $t = 4.5$ and 5 s, reduces the minimum local pressure above the peak. As the surface tension is reduced to 0.000576 N/m, the initial evolution of the perturbation wave is the same as $\sigma = 0.000993$ N/m. When the perturbation wave amplitude increases, the perturbation wave is reversed backward, resulting in the formation of finger structures. These structures were reported by Hou [31] and Tauber et al.[28]. At $t = 5$ s, some vortices move from the peak of the wave and are placed in front of the finger-shaped structure. These vortices are relatively weak and dissipated rapidly. At a later time, $t = 5.5$ s, the vortices are released again from the fingers. In this case, the instability at the interface grows with a larger amplitude than in the previous state due to the weaker effect of surface tension. As the shear layer thickens is enhanced, surface tension eventually pushes the interface forward, causing vortices to remain and move through both fluids ($t = 6$ s). This is due to the vortex shedding from the finger-shaped part of the interface. When $\sigma = 0.000288$ N/m, the fluid that accumulates at the tip of each finger forms a drop. The drop is attached to the rest of the finger by a thin string ($t = 5.5$ s) and in some cases, the drop is completely detached ($t = 6.5$ s). The best time to release the vortices from the finger is when the peak of the finger-shaped part of the interface turns forward. At intervals of 5 and 6 s, the vortices released from the finger-shaped part are more stable than the ones created at the initial time. For $\sigma = 0.000192$ N/m, the effect of a small amount of surface tension can be observed at $t = 5$ s, causing the highest part of the wave to be pulled more and move towards the finger, leading

to the creation of clockwise vortices inside the wave. At $t = 6$ and 5.5 s, the wave is a finger-shaped part of the interface is the same as in the previous cases.

The difference between the maximum and minimum distances of the wave from each other is calculated by the following relation:

$$A(t) = \frac{Y_{max} - Y_{min}}{2} \quad (17)$$

Fig. 5 illustrates $A(t)$ normalized by wavelength versus dimensionless time for different surface tensions. The figure reveals that dimensionless amplitude is the same for different surface tensions for $t^* \leq 1.5$. . Therefore, for $t^* > 1.5$ and this range of surface tension, the growth rate of KHI depends on the surface tension.

Two cases are explained by comparing Figs. 4 and 5. For $\sigma = 0.000993$ N/m, after the initial time ($t^* = 1.5$), the KHI begins and the amplitude decreases. Then, as the saltwater moves towards the right, the amplitude is increased. At $t^* = 2$, when the vortex shedding from the peak of the wave occurs, followed by the weakening of the shear rate and surface tension, normalized amplitude becomes maximum. Then, the motion of the wave to the right causes another fluid to place on the wave and push it. Thus, the amplitude of the wave is reduced and has a downward trend until the last dimensionless time. When the surface tension coefficient is 0.000576 N/m, the wave is growing until $t^* = 1.7$. The amplitude decreases with the formation of the wave and then the oscillations continue with the movement of the lower fluid to the left. At $t^* = 2$, when the vortex sheds from the wave peak and the consequent weakening of the shear rate, the amplitude decreases and will decline until $t^* = 2.15$, after which the wave continues to fluctuate.

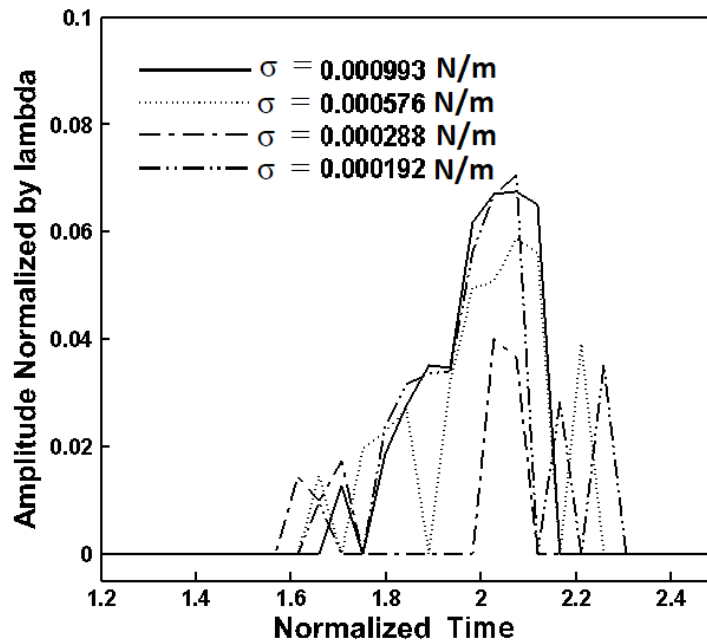


Fig. 5. Normalized $A(t)$ as a function of dimensionless time for different values of surface tension for $r = 0.93$, $m = 0.79$, $Re_1 = 1.49$, and $Re_2 = 1.19$.

4- 4- KHI of non-Newtonian fluids

In this section, KHI of non-Newtonian fluids is considered, when $k_1 = 0.04$, $k_2 = 0.01$, and $r = 1.08$.

4- 4- 1- Effect of power-law index

The rheology of non-Newtonian fluids is determined by the power-law equation [32]. In this section, the KHI of shear-thinning ($n < 1$) and shear-thickening ($n > 1$) non-Newtonian fluids are evaluated when $r = 1.08$. The characteristic of shear-thinning fluids is such a way that the rate of deformation increases with the strain rate. In other words, the viscosity of these fluids decreases by increasing the strain rate. But, shear-thickening fluids behave in contrast to shear-thinning ones so that their deformation rate decreases with the strain rate. In other words, the viscosity of these fluids increases by increasing the strain rate.

Figs. 6a, b, and c illustrate the Fourier analysis of the horizontal velocity at the interface between $t = 1.4$ s and $t = 3$ s for $n = 0.2, 0.4$, and 0.8 , respectively. Fourier transforms are obtained using FFT algorithm. Fig. 6a shows that similar to Newtonian fluids, the instability increases up to 1.8 s when the wavelength is 20 mm. After that, the instability decreases and then increases again and reaches a wavelength of 22 mm when $t > 2$. When the wavelength reaches 32 mm, the curves increase sharply, indicating that the interface does not change significantly. In addition, the matching of the critical wavelength with the most unstable wavenumber can be evaluated at 20 mm, where the critical wave number is 314.2 m. The amplitude of the critical waves can be considered as $\lambda_{cr} = 18-22$ mm. In Fig. 6b, the Fourier analysis is plotted for the

horizontal velocity at the interface between $t=1.4$ s and $t=3$ s for $n = 0.4$. This figure shows that there is instability in the interface up to a wavelength of 26 mm. After that, the curves increase sharply, indicating that the interface does not change significantly. The matching of the critical wavelength with the most unstable wavenumber can be evaluated at 18 mm, where the critical wave number is 349.1 m. The amplitude of the critical waves is in the range of $\lambda_{cr} = 16-22$ mm. Fig. 6c shows the Fourier analysis of the horizontal velocity at the interface between $t = 1.4$ s and $t = 3$ s for $n = 0.8$. The figure reveals that there is instability in the interface up to 22 mm wavelength. After that, the interface does not change significantly. Besides, the matching of the critical wavelength with the most unstable wavenumber can be evaluated at 16 mm (the critical wave number is 392.7 m). The amplitude of the critical waves is $\lambda_{cr} = 16-22$ mm.

In general, for shear-thinning non-Newtonian fluids, it can be concluded that the amount of wavelength after which the interface does not change decreases with the power-law index. Also, as n is enhanced, the critical wave number increases.

Figs. 7a, b, and c show the Fourier analysis of the horizontal velocity at the interface between $t = 1.4$ s and $t = 3$ s for $n = 1.2, 1.6$, and 1.8 , respectively. Fig. 7a shows that there is instability in the interface up to a wavelength of 22 mm. After that, the interface does not change significantly. The matching of the critical wavelength with the most unstable wavenumber can be evaluated at 14 mm, where the critical wave number is 448.8 m. The amplitude of the critical waves can be considered a $\lambda_{cr} = 12-16$ mm. In Fig. 8b, the Fourier

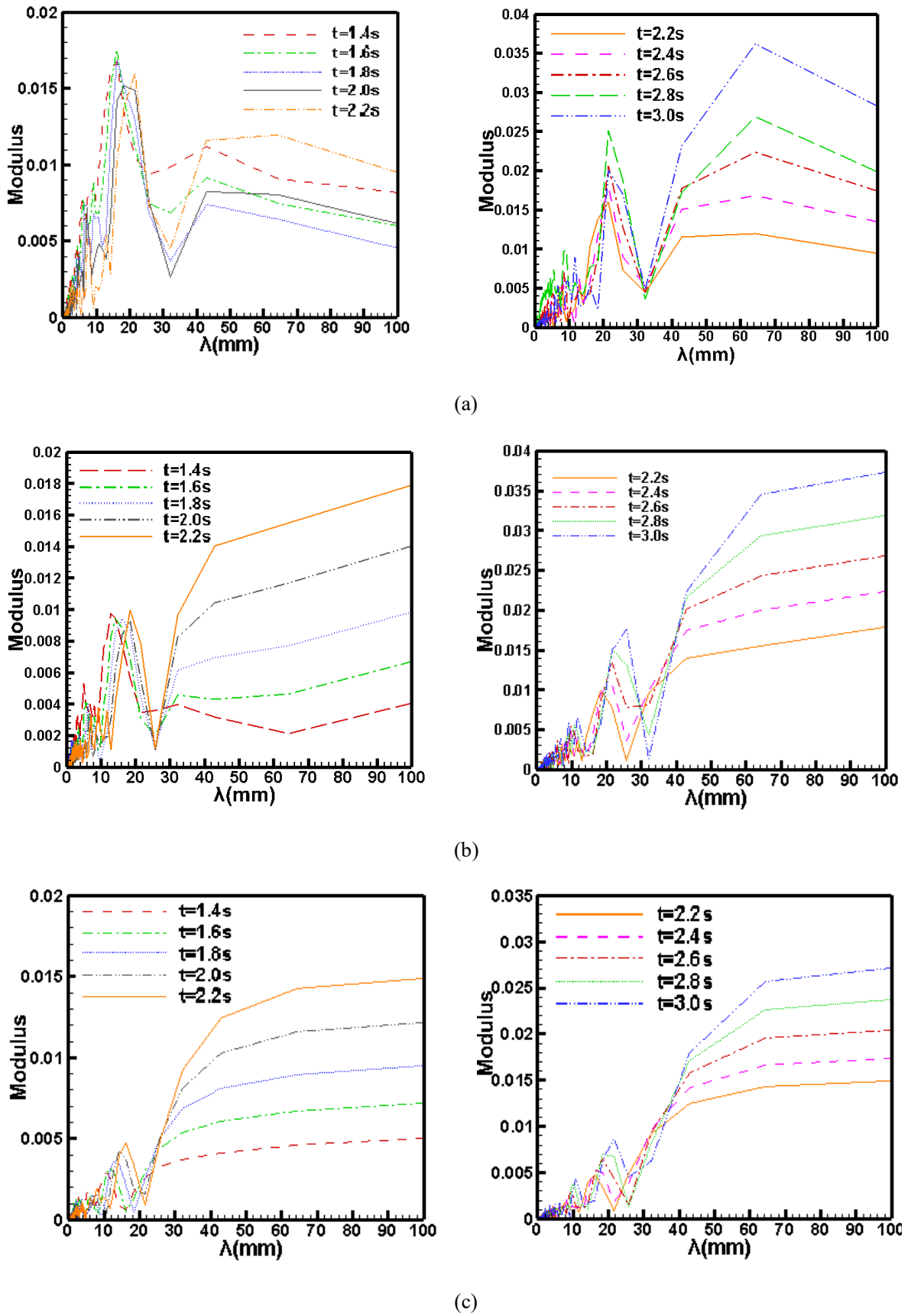
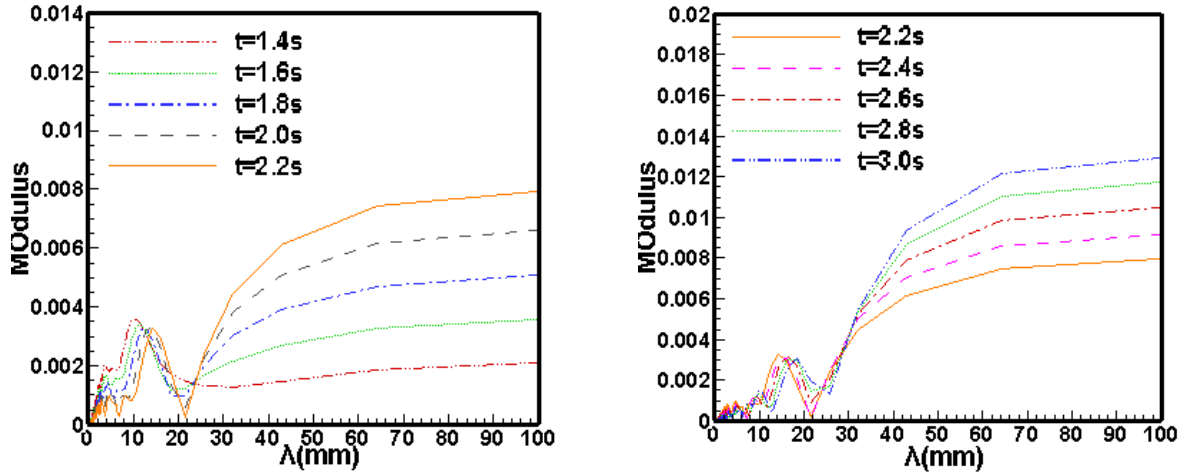
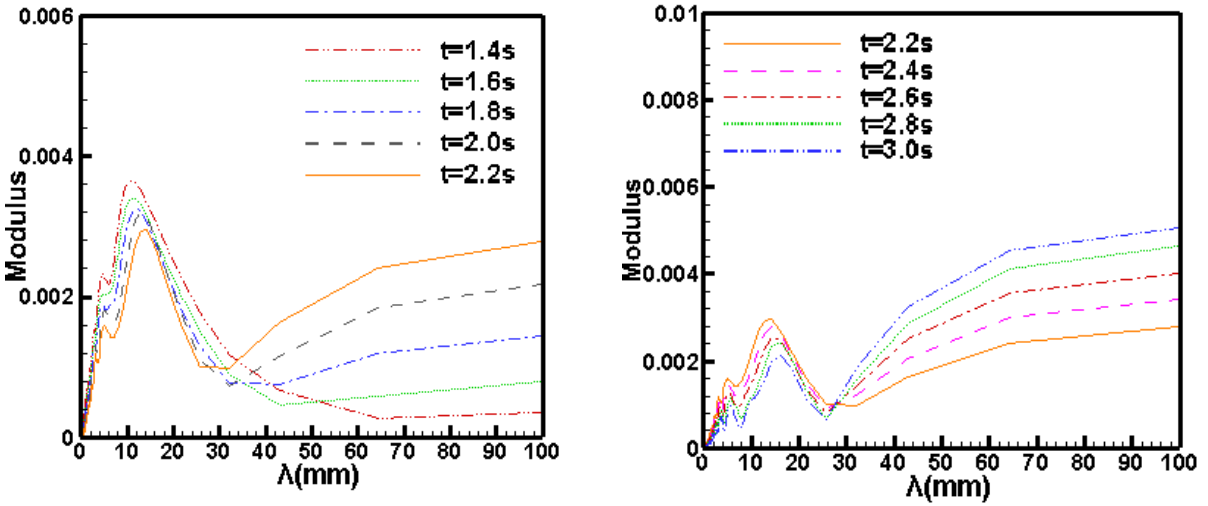


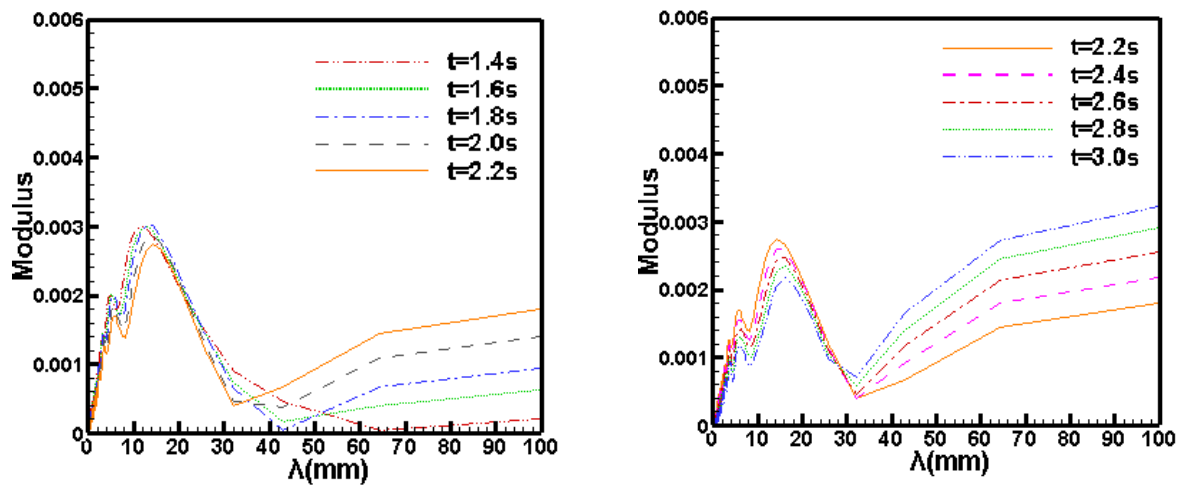
Fig. 6. Fourier analysis of the horizontal velocity at the interface versus wavelength between $t = 1.4$ s and $t = 3$ s for (a) $n = 0.2$, (b) $n = 0.4$, and (c) $n = 0.8$.



(a)



(b)



(c)

Fig. 7. Fourier analysis of the horizontal velocity at the interface versus wavelength between $t = 1.4$ s and $t = 3$ s for (a) $n = 1.2$, (b) $n = 1.6$, and (c) $n = 1.8$.

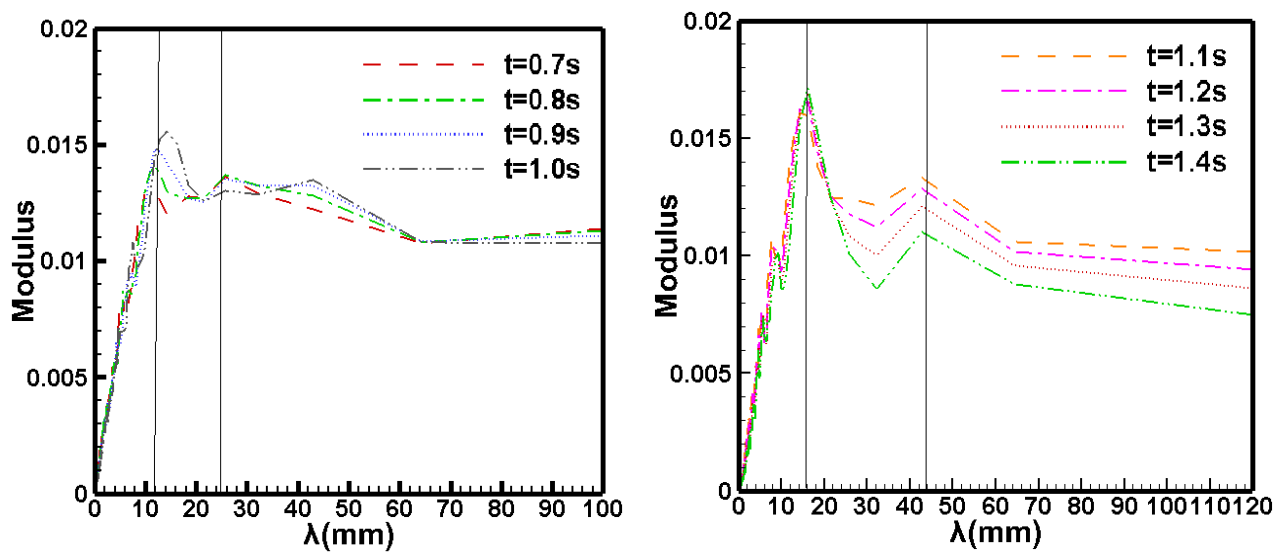


Fig. 8. Fourier analysis of the horizontal velocity at the interface versus wavelength between $t = 0.7$ s and $t = 1.4$ s for $n = 0.2$ and $\sigma = 0.0$ N/m.

analysis of the horizontal velocity at the interface is plotted between $t = 1.4$ s and $t = 3$ s for $n = 1.6$. This figure shows that there is instability in the interface up to the wavelength of 26 mm. After that, the interface does not change considerably. The matching of the critical wavelength with the most unstable wavenumber can be evaluated at 12 mm (critical wave number is 523.6 m. The amplitude of the critical waves is in the range of $\lambda_{cr} = 12-14$ mm. Finally, Fig. 8c shows the Fourier analysis of the horizontal velocity at the interface between $t = 1.4$ s and $t = 3$ s for $n = 1.8$. The figure shows that there is instability in the interface up to 32 mm wavelength, but after that, the interface varies slightly. Also, the matching of the critical wavelength with the most unstable wavenumber can be evaluated at 14 mm, considering that the critical wave number is equal to 448.8 m. The amplitude of the critical waves can be considered as $\lambda_{cr} = 12-16$ mm.

In general, for shear-thickening non-Newtonian fluids, it can be concluded that the amount of wavelength after which the interface does not change increases with the power-law index.

4- 4- 2- Effect of surface tension

To evaluate the effect of surface tension on the KHI, four surface tensions of 0.04 N/m, 0.004 N/m, 0.0008 N/m, and 0 N/m are considered when $n = 0.2$. The linear inviscid theory states that the most unstable wavelength decreases by decreasing the surface tension. For 0 N/m, infinite wave numbers are possible. Fig. 8 shows the Fourier analysis of the horizontal velocity at the interface for $\sigma = 0$ N/m. In the beginning, the critical wavelength is 12 mm. Then, the second wave is generated with a wavelength of 25 mm. For $t > 1.1$ s, the two primary wavelengths are transmitted to higher

wavelengths of $\lambda_{cr} = 16$ mm and $\lambda_{cr} = 42$ mm.

The horizontal velocity of the interface relative to the chamber height is plotted for surface tensions of 0.004 N/m and 0.0008 N/m at several different times in Fig.9. For $\sigma = 0.004$ N/m, the velocity profile is asymmetric, indicating that the velocity of the lighter liquid increases significantly at a specific height of the chamber. However, the velocity of the heavier liquid remains almost unchanged. As the surface tension decreases, i.e. $\sigma = 0.0008$ N/m, the interface velocity profile exhibits symmetrical behavior.

5- Conclusions

The present paper analyzes the KHI of Newtonian and non-Newtonian fluids numerically. Liquids are assumed to be incompressible and immiscible and the flow is unsteady. The effect of surface tension and power-law index on KHI is investigated for shear-thinning and shear-thickening fluids. In the case of Newtonian fluids, the results reveal that dimensionless amplitude is the same for different surface tensions for $t^* \leq 1.5$ when $\sigma = 0.000993-0.000192$ N/m, indicating that the growth rate of KHI depends on the surface tension at $t^* > 1.5$. For shear-thinning non-Newtonian fluids, it is concluded that the amount of wavelength after which the interface does not change decreases with the power-law index. For shear-thickening non-Newtonian fluids, the results demonstrate that the amount of wavelength after which the interface does not change increases with the power-law index. When $n = 0.2$ and $\sigma = 0.004$ N/m, the velocity profile is asymmetric, showing that the velocity of the lighter liquid increases significantly at a specific height of the chamber. As the surface tension decreases, the interface velocity profile exhibits symmetrical behavior.

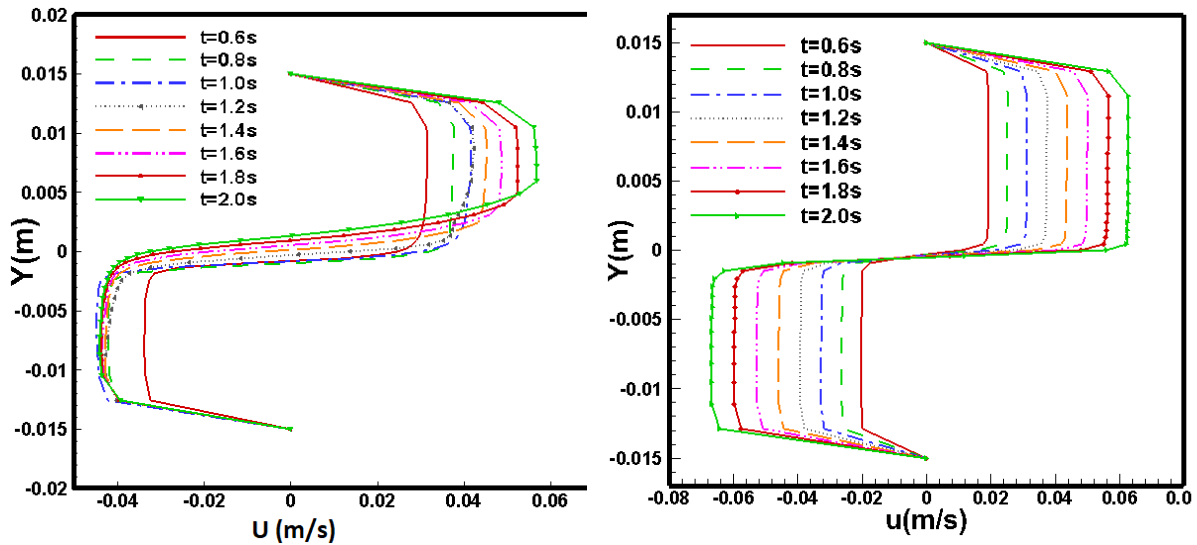


Fig. 9. Horizontal velocity versus height between $t = 0.6$ s and $t = 2.0$ s for $n = 0.2$ and (a) $\sigma = 0.004$ N/m and (b) $\sigma = 0.0008$ N/m.

References

- [1] P. Drazin, Kelvin–Helmholtz instability of finite amplitude, *Journal of Fluid Mechanics*, 42(2) (1970) 321-335.
- [2] H.v. Helmholtz, On discontinuous fluid motions, *Phil. Mag.*, 36(4) (1868) 337-346.
- [3] W.S. Thompson, Hydrokinetic solutions and observations, *Phil. Mag.*, (4) (1871) 374.
- [4] P. Hazel, Numerical studies of the stability of inviscid stratified shear flows, *Journal of Fluid Mechanics*, 51(1) (1972) 39-61.
- [5] S. Thorpe, A method of producing a shear flow in a stratified fluid, *Journal of Fluid Mechanics*, 32(4) (1968) 693-704.
- [6] S. Thorpe, Experiments on the instability of stratified shear flows: miscible fluids, *Journal of Fluid Mechanics*, 46(2) (1971) 299-319.
- [7] S. Thorpe, Turbulence in stably stratified fluids: A review of laboratory experiments, *Boundary-Layer Meteorology*, 5(1) (1973) 95-119.
- [8] S. Thorpe, Experiments on instability and turbulence in a stratified shear flow, *Journal of Fluid Mechanics*, 61(4) (1973) 731-751.
- [9] S. Thorpe, Transitional phenomena and the development of turbulence in stratified fluids: A review, *Journal of Geophysical Research: Oceans*, 92(C5) (1987) 5231-5248.
- [10] S.O. Unverdi, G. Tryggvason, A front-tracking method for viscous, incompressible, multi-fluid flows, *Journal of computational physics*, 100(1) (1992) 25-37.
- [11] P. Gondret, M. Rabaud, Shear instability of two-fluid parallel flow in a Hele–Shaw cell, *Physics of Fluids*, 9(11) (1997) 3267-3274.
- [12] S. Mohammadi Masiri, M. Bayareh, A. Ahmadi Nadooshan, Pairwise intercation of drops in shear-thinning inelastic fluids, *Korea-Australia Rheology Journal*, 31 (2019) 25-34.
- [13] H. Terashima, G. Tryggvason, A front-tracking/ghost-fluid method for fluid interfaces in compressible flows, *Journal of Computational Physics*, 228(11) (2009) 4012-4037.
- [14] L. Wang, W. Ye, W.-S. Don, Z. Sheng, Y. Li, X. He, Formation of large-scale structures in ablative Kelvin–Helmholtz instability, *Physics of Plasmas*, 17(12) (2010) 122308.
- [15] M.J. Chen, L.K. Forbes, Accurate methods for computing inviscid and viscous Kelvin–Helmholtz instability, *Journal of Computational Physics*, 230(4) (2011) 1499-1515.
- [16] I. Yilmaz, L. Davidson, F. Edis, H. Saygin, Numerical simulation of Kelvin-Helmholtz instability using an implicit, non-dissipative DNS algorithm, in: *Journal of Physics: Conference Series*, IOP Publishing, 2011, pp. 032024.
- [17] R. Zhang, X. He, G. Doolen, S. Chen, Surface tension effects on two-dimensional two-phase Kelvin–Helmholtz instabilities, *Advances in water resources*, 24(3-4) (2001) 461-478.
- [18] M.S. Shadloo, M. Yildiz, Numerical modeling of Kelvin–Helmholtz instability using smoothed particle hydrodynamics, *International Journal for Numerical Methods in Engineering*, 87(10) (2011) 988-1006.
- [19] M.K. Awasthi, G. Agrawal, Viscous contributions to the pressure for the potential flow analysis of magnetohydrodynamic Kelvin–Helmholtz instability, *International Journal of Applied Mechanics*, 4(01) (2012) 1250001.

- [20] S. Shiryaeva, A. Grigor'ev, S. Sukhanov, On the role of the viscosity of liquids in the realization of Kelvin-Helmholtz instability, *Surface Engineering and Applied Electrochemistry*, 49(5) (2013) 408-413.
- [21] J.E. Matsson, J. Boisselle, A Senior Design Project on the Kelvin-Helmholtz Instability, in: 2015 ASEE Annual Conference & Exposition, 2015, pp. 26.107. 101-126.107. 113.
- [22] M.K. Awasthi, Kelvin-Helmholtz instability of viscoelastic liquid-viscous gas interface with heat and mass transfer, *International Journal of Thermal Sciences*, 161 (2021) 106710.
- [23] Q.-f. Fu, X.-d. Deng, L.-j. Yang, Kelvin-Helmholtz instability of confined Oldroyd-B liquid film with heat and mass transfer, *Journal of Non-Newtonian Fluid Mechanics*, 267 (2019) 28-34.
- [24] J. Ghazanfarian, M. Moradi, Hybrid SPH-MD two-phase modelling of 3D free-surface flows introducing double KH instability, *Engineering Analysis with Boundary Elements*, 88 (2018) 115-131.
- [25] M. Esmailpour, M. Gholami Korzani, Analyzing Impacts of Interfacial Instabilities on the Sweeping Power of Newtonian Fluids to Immiscibly Displace Power-Law Materials, *Processes*, 9(5) (2021) 742.
- [26] M. Vadivukkarasan, Temporal instability characteristics of Rayleigh-Taylor and Kelvin-Helmholtz mechanisms of an inviscid cylindrical interface, *Meccanica*, 56(1) (2021) 117-124.
- [27] E. Berberovic, Investigation of free-surface flow associated with drop impact: numerical simulations and theoretical modeling, Technische Universität, 2010.
- [28] W. Tauber, S.O. Unverdi, G. Tryggvason, The nonlinear behavior of a sheared immiscible fluid interface, *Physics of Fluids*, 14(8) (2002) 2871-2885.
- [29] Z. Goodarzi, A.A. Nadooshan, M. Bayareh, Numerical investigation of off-centre binary collision of droplets in a horizontal channel, *Journal of the Brazilian Society of Mechanical Sciences and Engineering*, 40(3) (2018) 1-10.
- [30] C.W. Hirt, B.D. Nichols, Volume of fluid (VOF) method for the dynamics of free boundaries, *Journal of computational physics*, 39(1) (1981) 201-225.
- [31] T.Y. Hou, J.S. Lowengrub, M.J. Shelley, The long-time motion of vortex sheets with surface tension, *Physics of Fluids*, 9(7) (1997) 1933-1954.
- [32] M. Bayareh, S. Mortazavi, Numerical simulation of the motion of a single drop in a shear flow at finite Reynolds numbers, *Iranian Journal of Science and Technology Transaction B-Engineering*, 33 (2009) 441-452.

HOW TO CITE THIS ARTICLE

R. Farajzadeh, M. Bayareh, *Numerical Study of Kelvin-Helmholtz Instability of Newtonian and Non-Newtonian Fluids*, *AUT J. Mech Eng.*, 6 (2) (2022) 249-260.

DOI: [10.22060/ajme.2021.20382.5996](https://doi.org/10.22060/ajme.2021.20382.5996)

